DFG-Research Training Group "NatRiskChange"

Task Force on the 2023 Türkiye Earthquake Sequence

Behnam Maleki Asayesh[1,2,3], Thoralf Dietrich[1,2], Chen-Ray Lin[1,2,3]

[1]Institute of Environmental Science and Geography, University of Potsdam, Potsdam, Germany

[2]Institute of Geosciences, University of Potsdam, Potsdam, Germany

[3]Helmholtz Centre Potsdam, GFZ German Research Centre for Geosciences, Potsdam, Germany

Introduction

On 6 February 2023 at 04:17 local time (01:17 UTC), a M_W 7.8 earthquake struck southeastern Türkiye and northwestern Syria along the East Anatolian Fault (EAF) system with the epicenter close to the Turkish city Kahramanmaraş (Fig. 1; Gökkaya, 2016; Petersen et al., 2023). Around nine hours later, a M_W 7.5 earthquake occurred 100 km north of the first event on the Sürgü–Çardak fault adjacent to the East Anatolian Fault near Elbistan (Zhe et al., 2023). The occurrence of two main events with similarly large magnitudes is a rare occurrence in seismology.

The Kahramanmaraş earthquake (M_W 7.8) is the largest in Türkiye since the 1939 M_W 7.8 Erzincan earthquake (Hussain et al., 2018). It is also one of the strongest earthquakes ever recorded in the Levant. The earthquake could be sensed as far as Egypt and the Black Sea coast of Türkiye. More than 30,000 aftershocks occurred in the three months that followed. The two main events (M_W 7.8 Kahramanmaraş and M_W7.5 Elbistan) caused widespread damage in an area of about 350,000 km^2, about the size of Germany.

An estimated 14 million people (16 % of Türkiye's population) were affected. The confirmed death toll in Türkiye was 53,537; estimates of the number of dead in Syria were between 5,951 and 8,476. It is the deadliest disaster in Turkish and Syrian modern history and the deadliest worldwide since the 2010 Haiti earthquake. Damages were estimated at US$148.8 billion in Türkiye (9 % of Turkey's GDP) and US$14.8 billion in Syria. Development experts from the United Nations estimated that about 1.5 million people were left homeless.

There is continued debate on how the two main events are related and whether the first event directly triggered the second earthquake. Therefore, our research focused on three key aspects of this doublet earthquake, presented and discussed in the following order: (I) static ground displacement, (II) felt intensities, and (III) aftershocks analysis.

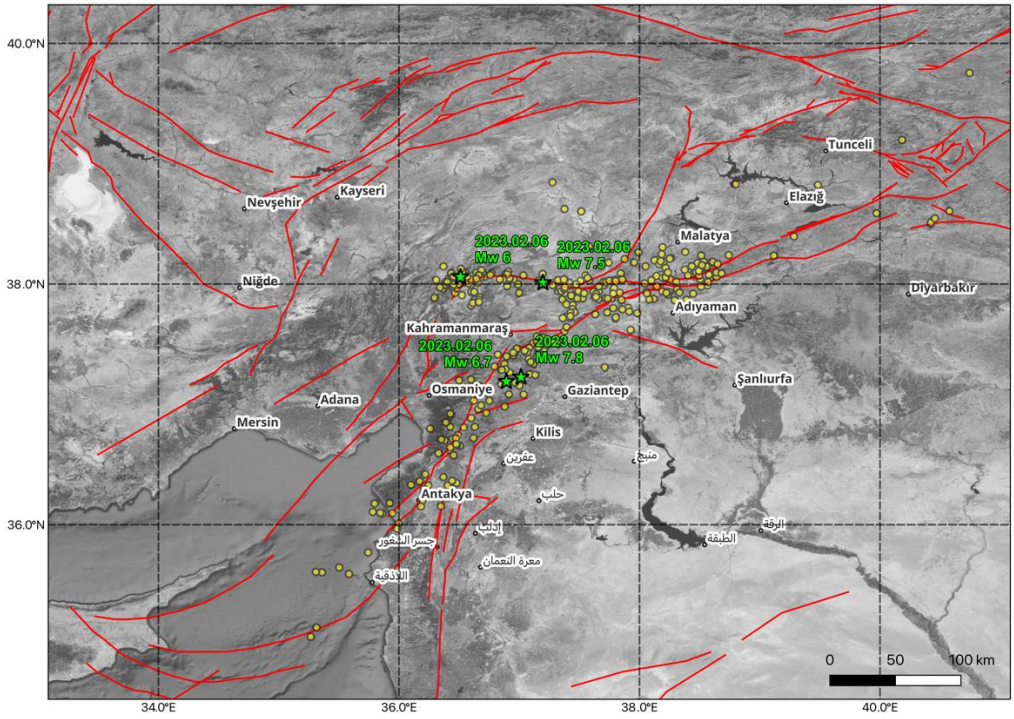

Figure 1. The seismicity map of the 2023 Türkiye earthquake sequence. Active faults (red lines data from Global Earthquake Model); epicenters of earthquakes from 29 January to 10 February 2023 (yellow circles, data from United States Geological Survey); epicenters of four major large events (M_W 6.0-7.8) in the sequence (green stars).

(I) Static ground displacement

Studying the potential for ground displacement can provide valuable insight into fault behavior, tectonic movement, and seismic hazards in a region. In this regard, we have estimated the static offsets that were triggered by four major events (M_W 6.0-7.8) during the 2023 Turkey earthquake sequence. We compute there-component static offsets with the inputs of the fault slip models of each major event from USGS based on the Okada (1985, 1992) model and project two horizontal static offsets along the flight track direction for the comparison with the Sentinel-1 InSAR records.

Figures 2a and 3a provide the fault slip distribution of the two main events across multiple segments (the MW7.8 Kahramanmaraş earthquake and the M_W 7.5 Elbistan earthquake). Additionally, Figures 2b and 2c demonstrate the estimated static offsets of the M_W 7.8 earthquake in the N-S and E-W components from fault slip distribution. The patterns indicate that the hanging wall (eastern side) was moving eastward and northward.

In Figures 2b-2c and 3b-3c, the two main events (M_W 7.8 and M_W 7.5) particularly caused strong static offsets when breaching the surface. However, while each event

caused offset, most of the affected area in the middle zone had offsets of opposing signs (Figures 4c-4d), thus resulting in relatively low net offset, as observed by InSAR (Figures 4a-4b), which only reveals the combined offset, while GPS and displacement inferred from accelerometers show large offsets for either event (Liu et al., 2023).

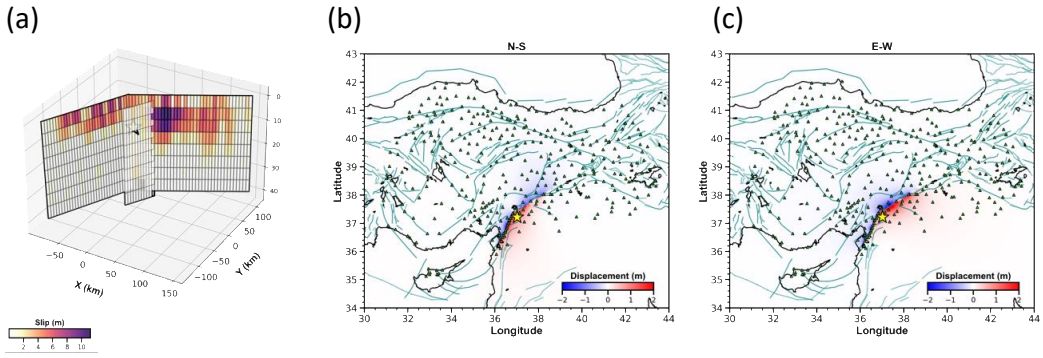

Figure 2. (a) Fault slip distribution of the M_W 7.8 mainshock on 6 February 2023, 01:17:35 UTC. (b, c) The estimated static offsets in two horizontal components (N-S and E-W direction, respectively) from the fault slip distribution.

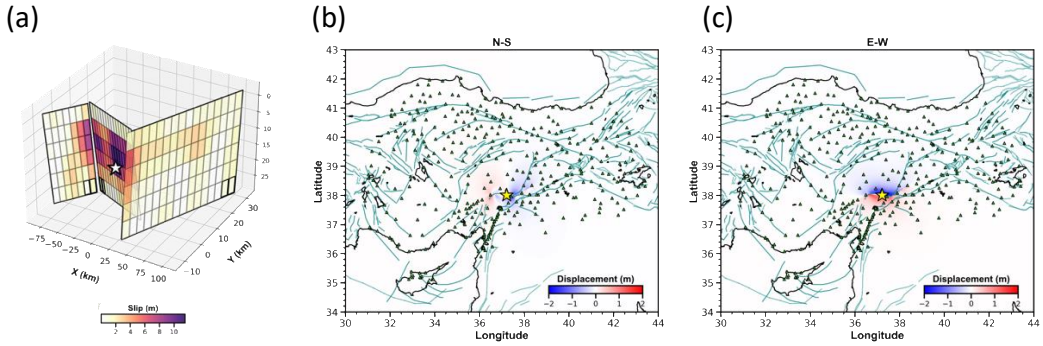

Figure 3. (a) Fault slip distribution of the M_W 7.5 earthquake on 6 February 2023, 10:24:50 UTC. (b, c) The estimated static offsets in two horizontal components (N-S and E-W direction, respectively) from the fault slip distribution.

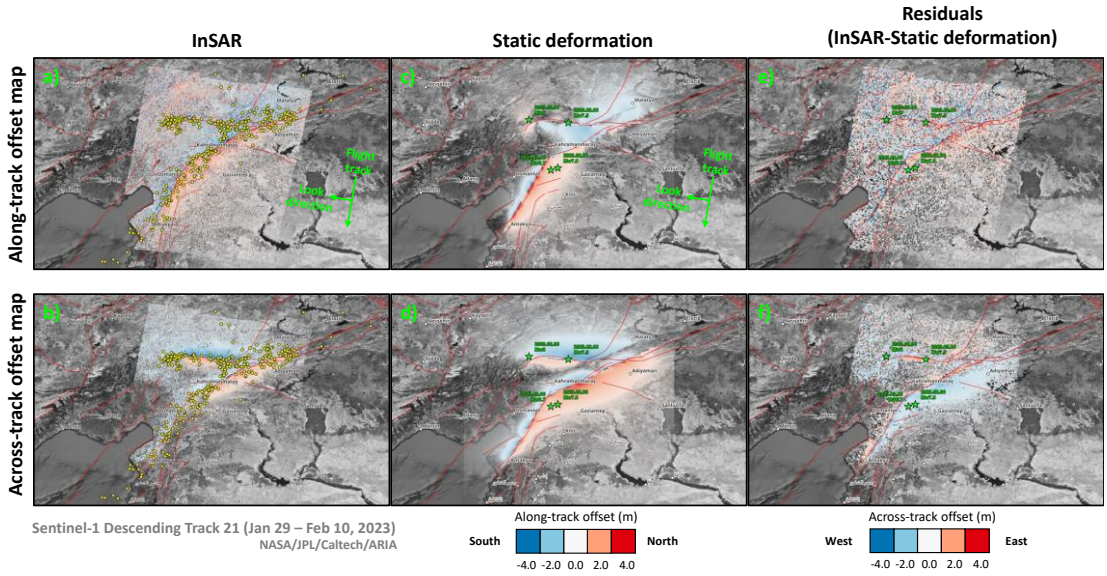

Figure 4. (a, b) Static offsets in the along-track and across-track directions derived from ESA Sentinel-1 radar image acquired on 28 January 2023 and 10 February 2023. Active faults (red lines); epicenters of earthquakes from 29 January to 10 February 2023 (yellow circles). (c, d) Total static offsets from the four major events of the earthquake sequence projected in the along-track and across-track directions. Epicenters of four major large events (MW 6.0-7.8) in the sequence (green stars). (e, f) Residuals between calculated and observed static offsets.

(II) Felt Intensities

The felt reports provide valuable information about how people experience earthquakes and augment essentially spatial points across a region affected by an earthquake. In other words, we use humans as "instruments." These data can be used to increase public engagement, understand the building damages from an earthquake, and validate instrumental data (e.g., strong-motion seismometer).

The previous section discussed the static offset after an earthquake. However, that is not the only wavefield of displacement occurring during an earthquake. Seismic waves pass through the regions and shake people, buildings, the earth, and everything anchored to the ground. When the forces are strong enough, structures are destroyed, causing permanent damage, which is strongly associated with acceleration.

The damage of the infrastructures is visible in satellite images (e.g., Sudhaus et al., pers. communication; Yu et al., 2024), but we can use strong-motion intensities from the Mercalli scale to look at the damage pattern during the earthquake. For instance in the Mercalli scale (Wood et Neumann, 1931; Dewey et al., 1995):

1. IX to X: total destruction of houses and everything
2. I to 0: barely perceived/ not felt at all.

We collected the felt reports from USGS and used a standard technique in psychology (due to questionnaires) and different class-based science to obtain different aspects into the distribution of the felt reports.

The multinomial logistic regression only needs well-ordered classes. This is the case with ever-increasing shaking and destruction in the Mercalli scale of earthquake reports. For a given set of data, the multinomial regression assigns probabilities to all dependent variables of the data points to which of the ordered classes they belong (Figures 6a and 8a) based on an explanatory variable. In the case of the felt Mercalli Scale, the distance explains the shaking. Therefore, for any given distance, the probabilities of the different classes average to a unique value, similar to an expected value.

In comparison to the "traditional" linear regression, the multinomial regression saturates with the end classes. The result is reasonable since you cannot destroy more than everything (Intensity 10) or less than nothing (Intensity 1—just above the detection limit). Therefore, we estimated residual intensities between the intensities from the original reports with the evaluated values of the multinomial logistic regression. The residuals indicate how well this theoretical intensity value fits the reported data. In the first order (6b and 8b), they show the extent of the whole fault, as strong shaking appears along the complete fault, not only at the epi- and hypocenter. However, in the second-order observations, the residual reported intensities are much higher in the East of the fault (underestimation of the intensity) than in the West for the first main shock, the Pazarcik earthquake (Figure 7b).

From the second mainshock, the pattern is not as clear as the first mainshock's pattern. However, a feature can be seen at the coast of the Black Sea. The rupture length was much shorter for this Elbistan earthquake, and the coast is more than 500 km away. Yet the reports around the City of Ordu (red dot at 41°N, 37°E) are much stronger than expected. This becomes less and less towards the East and West of the coast. This is directly north of the fault, coinciding with one lobe of the northward radiation pattern of S-waves.

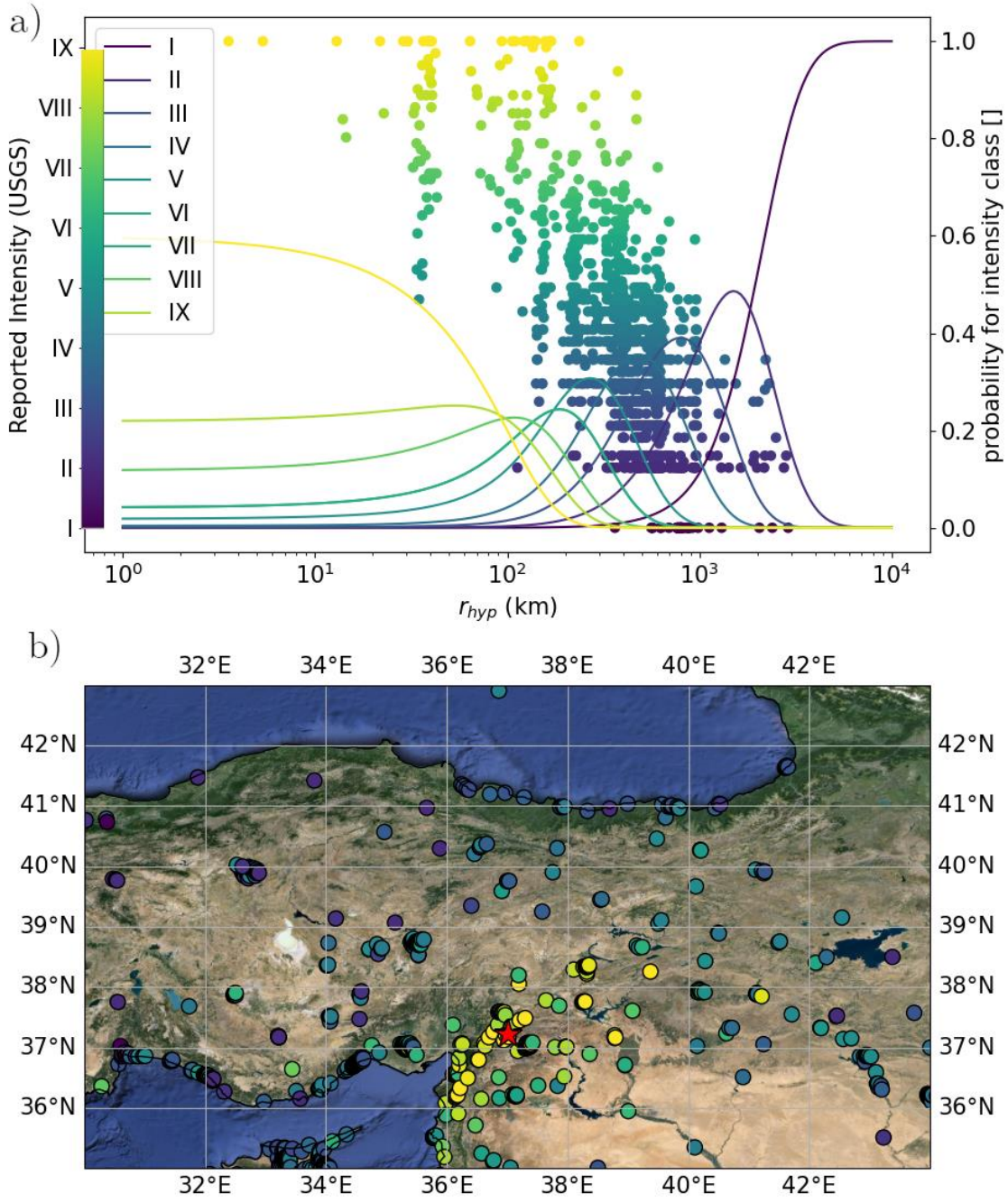

Figure 5. (a) Felt reports provided by the USGS for the first Mw 7.8 mainshock, the Pazarcik earthquake, plotted by distance versus felt intensity. The color (see colorbar at the left side) indicates strength. Also given are the corresponding intensity classes with their probability of fitting given the distance. (b) Map of the felt report distribution. The hypocenter is marked with a red star; the reports are coded by their intensity (see Figure 5a). The distribution of the largest magnitude (yellow colors) redraws the surface extent of the fault rupture.

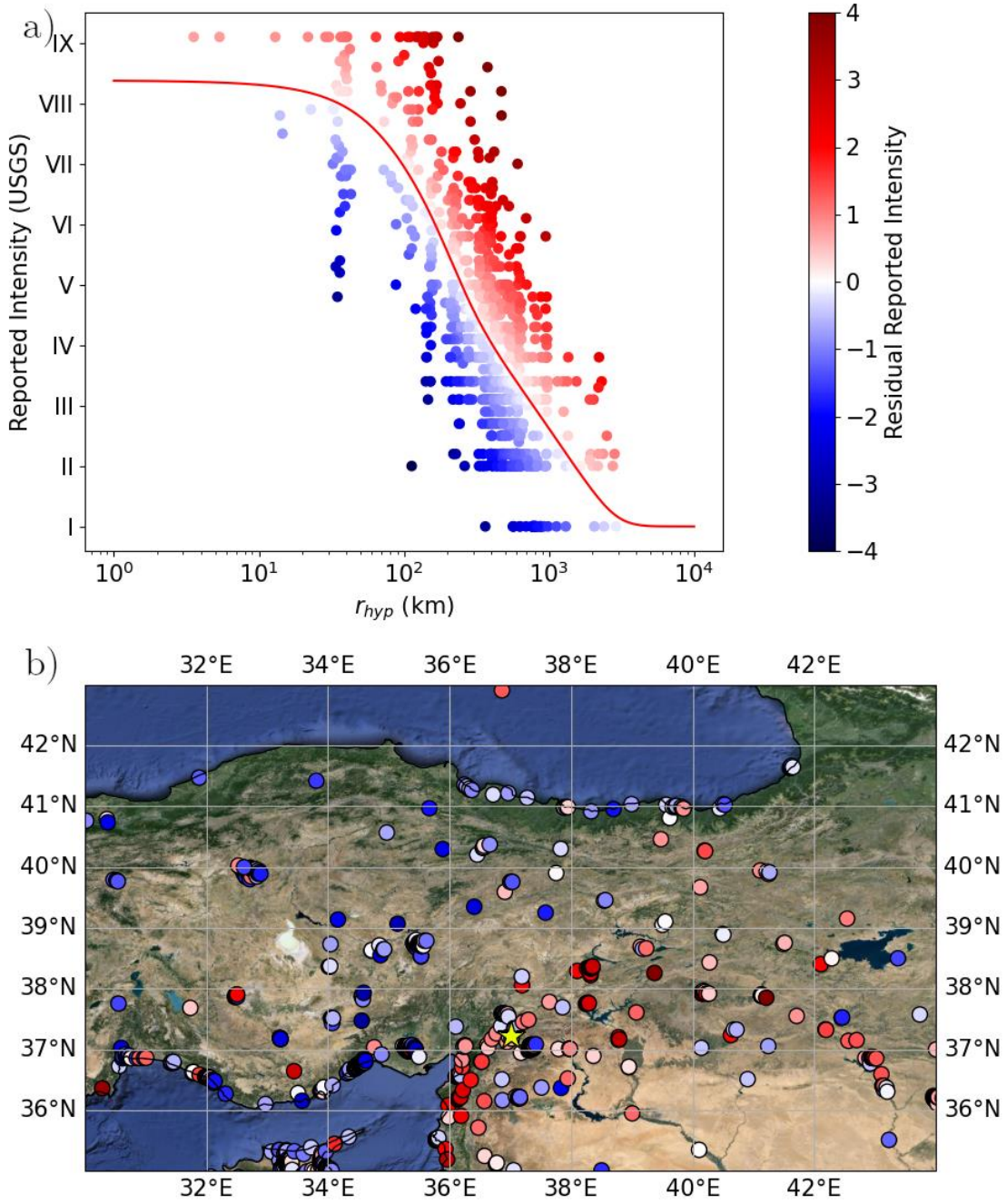

Figure 6. (a) The data of Figure 5a (Pazarik, 1st mainshock) is interpolated with the multinomial logistic regression. The reports are coded by their residuals, i.e., the difference between interpolated and reported intensity. The colors are the same in both subplots. (b) The data on the map is also coded by residuals.

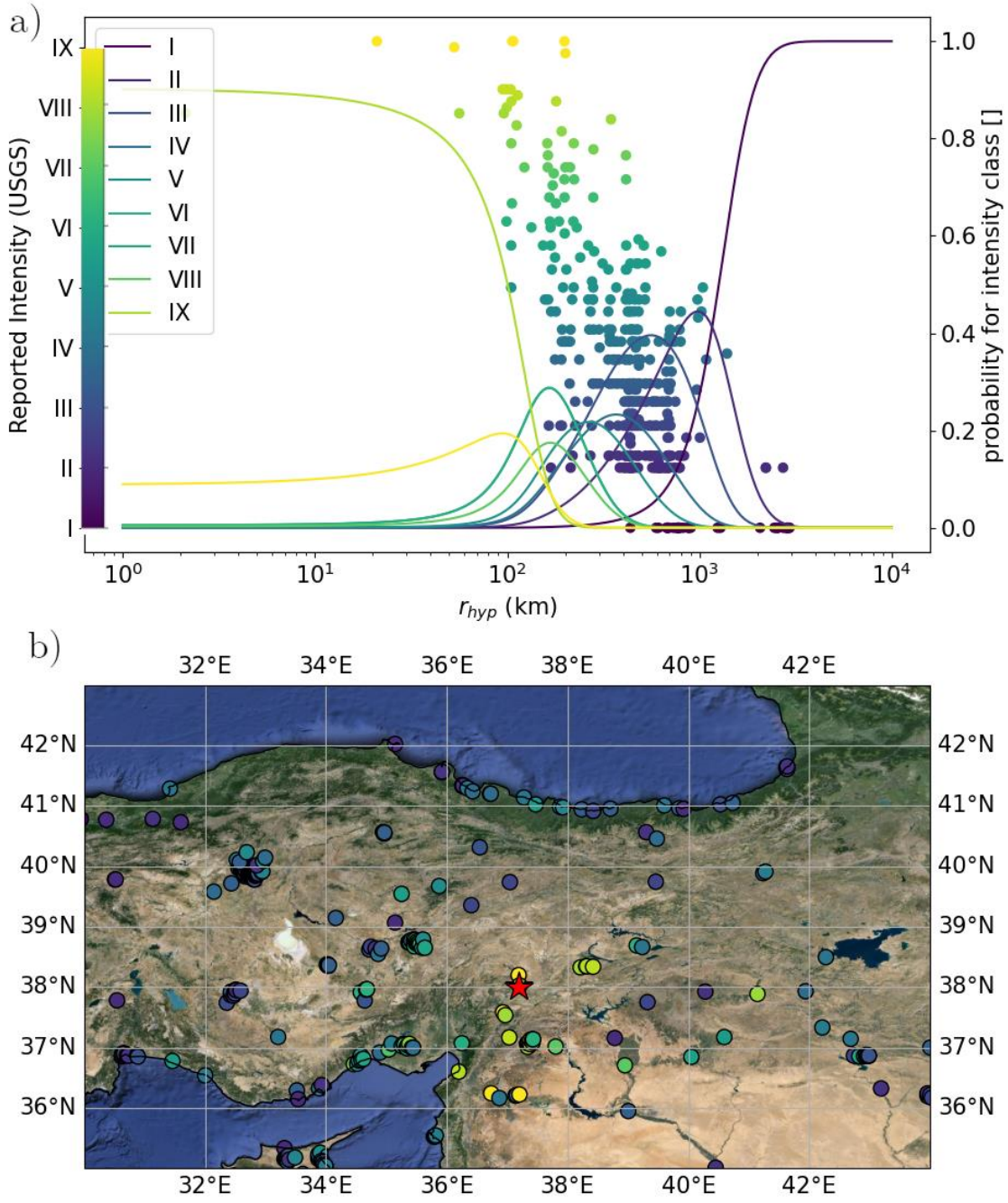

Figure 7. a) Felt reports of the second main shock, the Elbistan earthquake, sorted by hypocentral distance. The color (see colorbar at the side) indicates the strength of the reports. Also given are the corresponding Intensity classes with their probability to fit given the distance. b) Map distribution of the felt reports. The total amount of reports is lower than for the first shock. The red star marks again the hypocentre. For the second shock, the fault however can not be traced back on results alone.

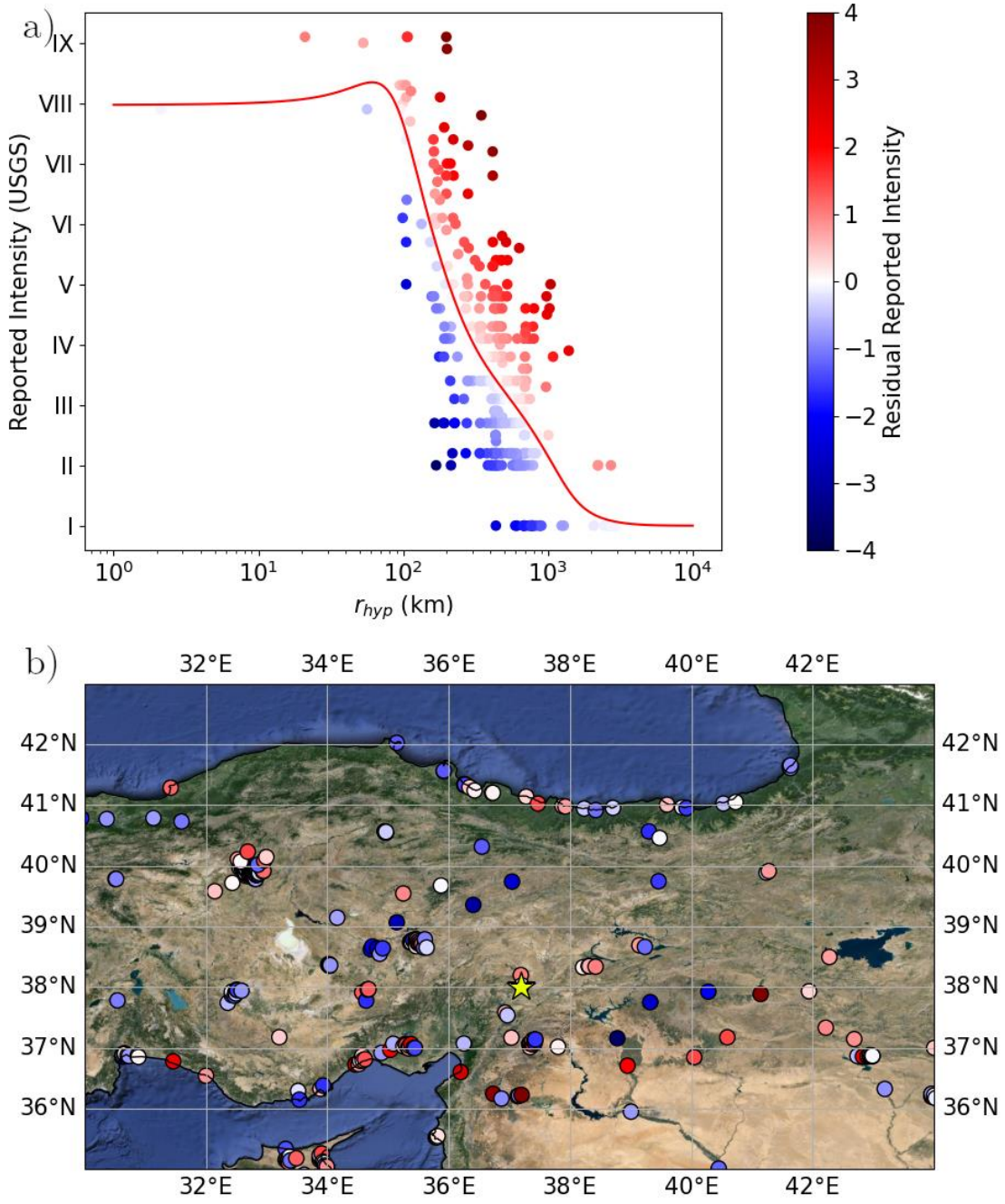

Figure 8. (a) The data (Elbistan earthquake) of Figure 8a is interpolated with the multinomial logistic regression. The reports are coded by their residuals, i.e., the difference between interpolated and reported intensity. The colors are the same in both subplots. (b) The data on the map is also coded by residuals.

(III) Aftershocks analysis

Large earthquakes permanently alter the stress in nearby faults. These stress changes can trigger a sequence of aftershocks. Sometimes, these aftershocks can be as destructive or deadly as the mainshock or even worse, such as the Christchurch event

that was triggered by the Darfield mainshock (Stramondo et al., 2011) or this sequence that occurred recently in Türkiye. Due to the destructive potential of aftershocks, an accurate probabilistic forecast of the spatial and temporal distribution of aftershocks is of utmost importance for rescue planning, emergency decision-making, and risk mitigation in the affected area.

While the spatial distribution of aftershocks is more difficult to explain and predict, their temporal decay is well described by the Omori law (Utsu, 1961). Perhaps the static stress transfer hypothesis is the most widely accepted and used criterion to explain aftershocks triggering and their spatial pattern (e.g. King et al. 1994; Toda et al. 1998; Asayesh et al. 2020). Recently, some studies have shown that number of alternative scalar metrics such as Coulomb stress changes (ΔCFS) calculated for variable mechanism (VM), maximum shear (MS), and von Mises stress (VMS) are better predictors of aftershock locations (e.g., Meade et al., 2017; Sharma et al., 2020; Asayesh et al., 2023). In this regard, we do some statistical analysis of aftershocks and investigate the correlation of aftershocks spatial distribution and stress scalars.

The 2023 Kahramanmaraş doublets triggered intense seismicity in their epicentral area. About 55000 earthquakes ($M_W \geq 0$) were recorded by AFAD by the end of the year (Figure 9). More than 20000 events had a magnitude equal to or greater than 2. In addition to the mainshocks, a M_W 6.4 magnitude aftershock occurred on 20 February near Antakya in the southwest.

We started with a statistical analysis and selected all events that occurred by the end of 2023 within the poly buffer area (dashed green line in Figure 9). This dataset consists of about 55000 aftershocks recorded by AFAD with magnitudes ranging from 0-7.7. Although some of these events were probably unrelated to the main earthquake, we consider them all aftershocks. Figure 10a shows the temporal occurrence and the frequency–magnitude distribution of the selected events. The depth distribution of these events is less than 20 km with a concentration of 7 km (Figure 10b). We estimated the completeness magnitude (Mc) of the dataset using two different standard procedures. The fast and straightforward ‘maximum curvature method’ (Wyss et al., 1999; Wiemer & Wyss, 2000), which defines Mc by the maximum of the magnitudes’ histogram, yields a completeness magnitude of 1.5. Using the Ogata and Katsura (1993) model that considers a detection probability function to fit the entire magnitude range (EMR) yields a Mc value of 1.8 and 2.1 for a 90 and 99 percent confidence level, respectively (Figure 10c). Our analysis considered events with magnitudes equal to or greater than 2.

T The next step was to estimate the Omori parameters for our database ($M_W \geq 2$) using a maximum likelihood function. Figure 11 shows aftershock rates with time and estimated parameters. It shows that the activity of aftershocks for the 2023 Türkiye

sequence decays in time according to a power-law distribution.

In the last step, we used the slip models calculated by Barbot et al. (2023) for the Kahramanmaraş doublets and the Antakya aftershock and calculated the Coulomb stress changes on the main fault mechanism (MAS), Coulomb stress changes on the variable mechanism (VM), maximum shear stress (MS) and von Mises stress (VMS) to check the correlation between the spatial distribution of the aftershocks and the stress patterns (Figure 12). Our results confirm the correlation between stress scalar and aftershocks spatial distribution, particularly for VM, MS, and VMS.

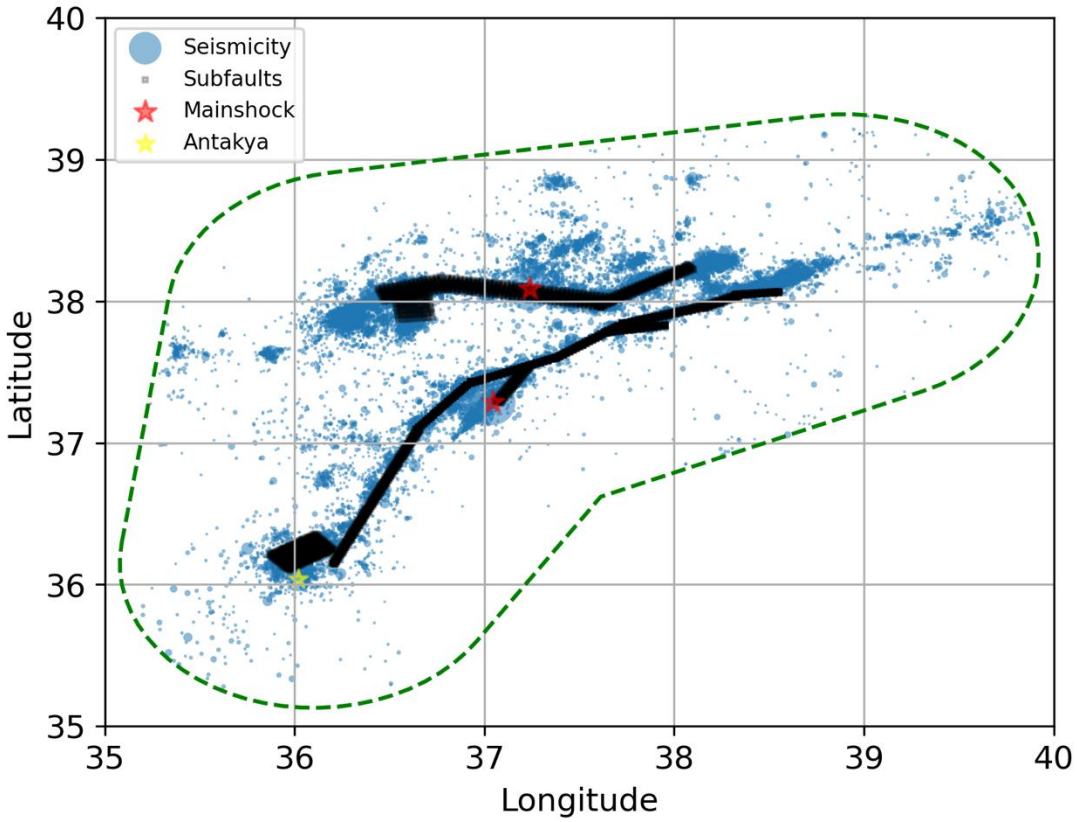

Figure 9. Epicentral distribution of the mainshocks (Kahramanmaraş doublets, red stars) and the Antakya aftershock (yellow star) and their subsequent seismicity (circles) from the AFAD catalog ($M_W \geq 0$). The squares show the subfaults introduced by Barbot et al. (2023) for slip models of these events. The dashed green line encircles the events selected in this study.

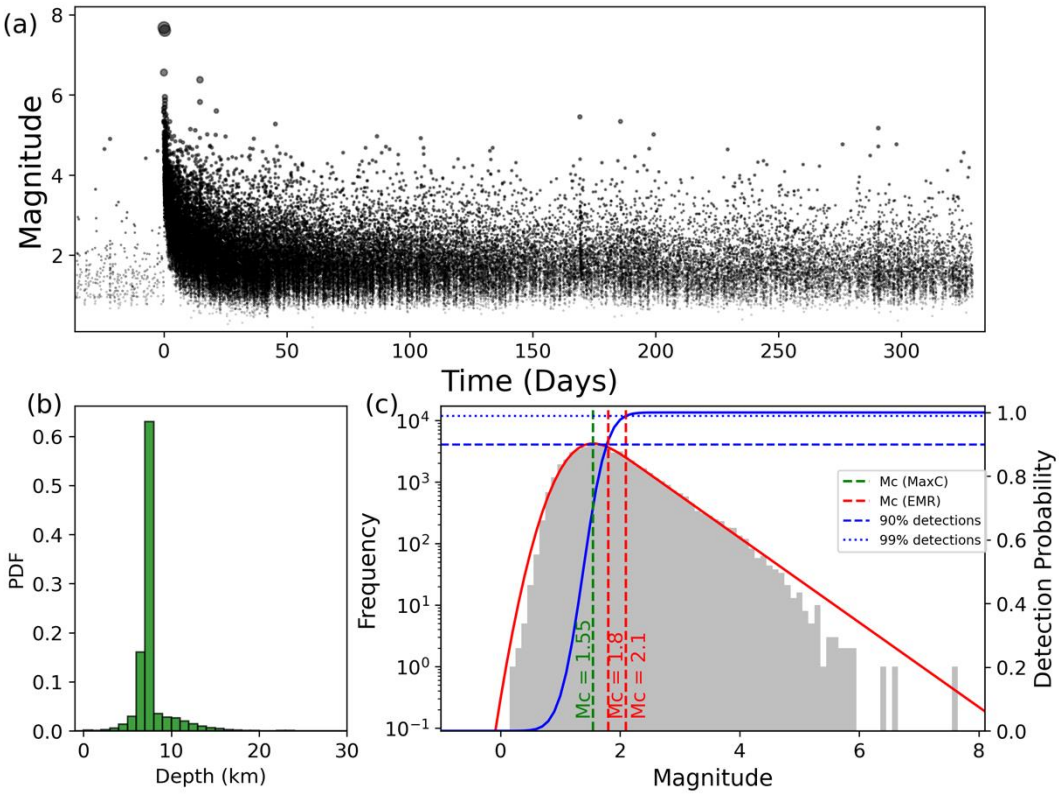

Figure 10. (a) Magnitude versus time plot of events that occurred within the selected poly buffer by the end of 2023. (b) Probability density function of the depth distribution of these events. (c) Noncumulative frequency–magnitude distribution, where the completeness magnitude (Mc) is estimated as 1.55 according to the maximum curvature (MaxC) method, while the fit of the Ogata and Katsura (1993) model (solid lines) yields 1.8 and 2.1 for detection probabilities of 90 and 99 percent (dotted horizontal lines), respectively.

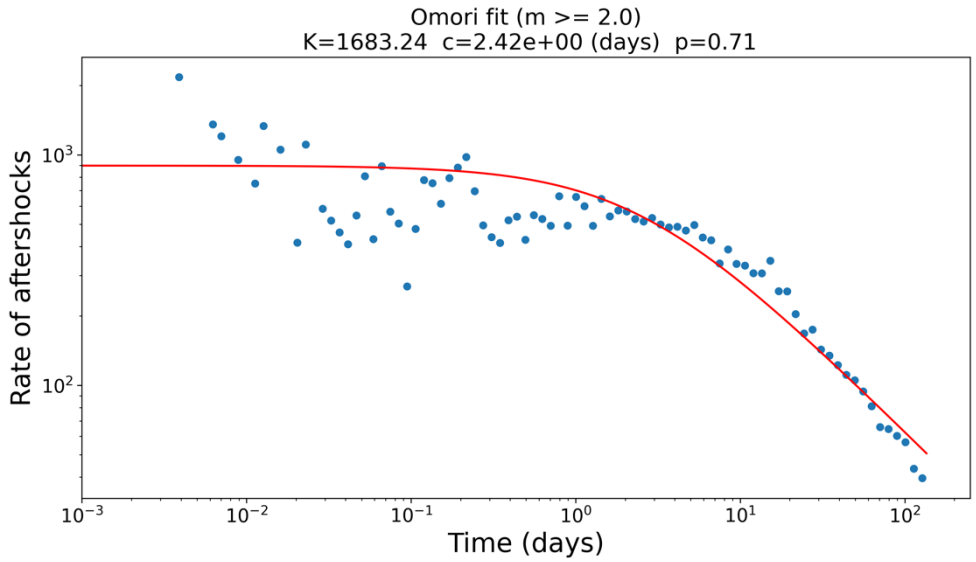

Figure 11. Estimated Omori parameters using a maximum likelihood function and fitting it to the dataset ($M_W \geq 2$).

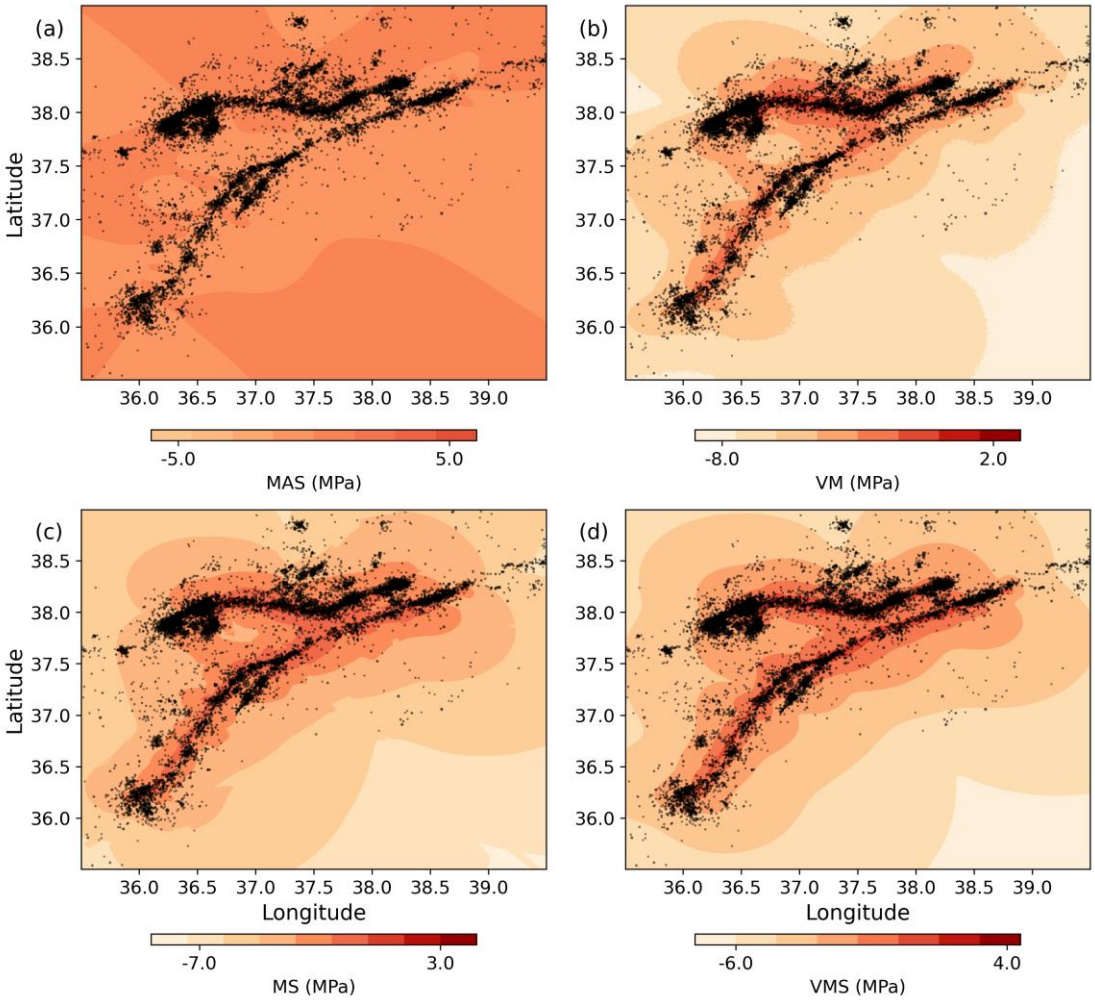

Figure 12. (a) Coulomb stress change on main fault (MAS), (b) log of Coulomb stress on variable mechanism (VM), (c) log of maximum shear stress (MS), and (d) log of von Mises stress (VMS). All plotted stress scalars are calculated at the depth of 7.5 km. Black dots show seismicity at depths between 7 and 8 km.

References

[1] Asayesh, B. M., Zafarani, H., Hainzl, S., & Sharma, S. (2023). Effects of large aftershocks on spatial aftershock forecasts during the 2017–2019 western Iran sequence. Geophysical Journal International, 232(1), 147-161.

[2] Asayesh, B. M., Zafarani, H., & Tatar, M. (2020). Coulomb stress changes and secondary stress triggering during the 2003 (Mw 6.6) Bam (Iran) earthquake. Tectonophysics, 775, 228304.

[3] Barbot, S., Luo, H., Wang, T., Hamiel, Y., Piatibratova, O., Javed, M. T., ... & Gurbuz, G. (2023). Slip distribution of the February 6, 2023 Mw 7.8 and Mw 7.6, Kahramanmaraş, Turkey earthquake sequence in the East Anatolian fault zone. Seismica, 2(3).

[4] Gökkaya, K. (2016). Geographic analysis of earthquake damage in Turkey between 1900 and 2012. Geomatics, Natural Hazards and Risk, 7(6), 1948-1961.

[5] Hussain, E., Wright, T. J., Walters, R. J., Bekaert, D. P., Lloyd, R., & Hooper, A. (2018). Constant strain accumulation rate between major earthquakes on the North Anatolian Fault. Nature communications, 9(1), 1392.

[6] Jia, Z., Jin, Z., Marchandon, M., Ulrich, T., Gabriel, A. A., Fan, W., ... & Fialko, Y. (2023). The complex dynamics of the 2023 Kahramanmaraş, Turkey, M w 7.8-7.7 earthquake doublet. Science, 381(6661), 985-990.

[7] King, G. C., Stein, R. S., & Lin, J. (1994). Static stress changes and the triggering of earthquakes. Bulletin of the Seismological Society of America, 84(3), 935-953.

[8] Liu, C., Lay, T., Wang, R., Taymaz, T., Xie, Z., Xiong, X., ... & Erman, C. (2023). Complex multi-fault rupture and triggering during the 2023 earthquake doublet in southeastern Türkiye. Nature Communications, 14(1), 5564.

[9] Meade, B. J., DeVries, P. M., Faller, J., Viegas, F., & Wattenberg, M. (2017). What is better than Coulomb failure stress? A ranking of scalar static stress triggering mechanisms from 105 mainshock-aftershock pairs. Geophysical Research Letters, 44(22), 11-409.

[10] Ogata, Y., & Katsura, K. (1993). Analysis of temporal and spatial heterogeneity of magnitude frequency distribution inferred from earthquake catalogues. Geophysical Journal International, 113(3), 727-738.

[11] Okada, Y. (1985). Surface deformation due to shear and tensile faults in a half-space. Bulletin of the seismological society of America, 75(4), 1135-1154.

[12] Okada, Y. (1992). Internal deformation due to shear and tensile faults in a half-space. Bulletin of the seismological society of America, 82(2), 1018-1040.

[13] Petersen, G. M., Büyükakpinar, P., Vera Sanhueza, F. O., Metz, M., Cesca, S., Akbayram, K., ... & Dahm, T. (2023). The 2023 Southeast Türkiye seismic sequence: rupture of a complex fault network. The Seismic Record, 3(2), 134-143.

[14] Sharma, S., Hainzl, S., Zöeller, G., & Holschneider, M. (2020). Is Coulomb stress the best

choice for aftershock forecasting?. Journal of Geophysical Research: Solid Earth, 125(9), e2020JB019553.

[15] Stramondo, S., Kyriakopoulos, C., Bignami, C., Chini, M., Melini, D., Moro, M., ... & Boschi, E. (2011). Did the September 2010 (Darfield) earthquake trigger the February 2011 (Christchurch) event?. Scientific reports, 1(1), 98.

[16] Toda, S., Stein, R. S., Reasenberg, P. A., Dieterich, J. H., & Yoshida, A. (1998). Stress transferred by the 1995 Mw= 6.9 Kobe, Japan, shock: Effect on aftershocks and future earthquake probabilities. Journal of Geophysical Research: Solid Earth, 103(B10), 24543-24565.

[17] Utsu, T. (1961). A statistical study on the occurrence of aftershocks. Geophys. Mag., 30, 521-605.

[18] Wiemer, S., & Wyss, M. (2000). Minimum magnitude of completeness in earthquake catalogs: Examples from Alaska, the western United States, and Japan. Bulletin of the Seismological Society of America, 90(4), 859-869.

[19] Wyss, M., Hasegawa, A., Wiemer, S., & Umino, N. (1999). Quantitative mapping of precursory seismic quiescence before the 1989, M 7.1 off-Sanriku earthquake, Japan. Annals of Geophysics, 42(5).

[20] Yu, X., Hu, X., Song, Y., Xu, S., Li, X., Song, X., ... & Wang, F. (2024). Intelligent assessment of building damage of 2023 Turkey-Syria Earthquake by multiple remote sensing approaches. npj Natural Hazards, 1(1), 3.

[21] https://earthquake.usgs.gov/earthquakes/eventpage/us6000jllz/dyfi/intensity, last accessed on May 13, 2024. No corresponding author given.

[22] Wood, H.O. and Neumann, F. (1931) Modified Mercalli Intensity Scale of 1931. Bulletin of the Seismological Society of America (1931) 21 (4): 277–283.

[23] Dewey, J. W., Reagor, B. G. , Dengler, L., Moley, K. (1995). Intensity Distribution and Isoseismal maps for the Northridge, California, Earthquake of January 17, 1994, USGS Open-File Report 95-92.